DTU Library

Impact of steam generator start-up limitations on the performance of a parabolic trough solar power plant

Ferruzza, Davide; Topel, Monika; Laumert, Björn; Haglind, Fredrik

Link back to DTU Orbit

1 # Impact of steam generator start-up limitations on the performance of a

2 # parabolic trough solar power plant

3 Davide Ferruzza[1], Monika Topel[2], Björn Laumert[2], Fredrik Haglind[1].

4 [1]Department of Mechanical Engineering, Technical University of Denmark, Nils Koppels Allé, Building
5 403, 2800 Kongens Lyngby, Denmark

6 [2]Department of Energy Technology, KTH Royal Institute of Technology, 100 44, Stockholm, Sweden

7 *Phone number: +45 27296900, e-mail: *daferr@mek.dtu.dk*

8 **Abstract**

9 Concentrating solar power plants are an attractive option in the renewable energy generation market. The

10 possibility of integrating relatively cheap forms of energy storage makes them a desirable solution when

11 power generation must be readily available at any time of the day. Solar power plants typically start-up

12 and shut down every day, so in order to maximize their profitability, it is necessary to increase their

13 flexibility in transient operation and to initiate power generation as rapidly as possible. Two of the key

14 components are the steam generator and steam turbine and the rates at which they can reach operational

15 speed are limited by thermo-mechanical constraints. This paper presents an analysis of the effects of the

16 thermal stress limitations of the steam generator and steam turbine on the power plant start-up, and

17 quantifies their impact on the economy of the system. A dynamic model of a parabolic trough power plant

18 was developed and integrated with a logic controller to identify start-up limitations, and subsequently the

19 dynamic model was integrated in a techno-economic tool previously developed by the authors. The plant

20 was analysed under two different operating strategies, namely solar-driven and peak-load. The results

21 indicate that for steam generator hot start-ups, a 1.5 % increase in peak-load electricity production would

22 be achieved by doubling the maximum allowable heating rate of the evaporator. No useful increase would

23 be achieved by increasing the rates beyond a limit of 7-8 K/min, as the turbine would then be the main

24   limiting component during start-up. Similar conclusions can be drawn for the solar-driven case, for which

25   the solar field and the energy source availability would pose the major constraint when starting up the

26   steam generator system.

27   ***Key words:*** *Solar Energy, Concentrating Solar Power, Parabolic Trough power plant; Steam generator;*

28   *Steam turbine; Start-up;*

29   **Nomenclature**

30   ACC   Air cooled condenser

31   CSPP   Concentrating Solar Power plant

32   CT   Cold tank

33   D   Deaerator

34   ECO   Economizer

35   EVA   Evaporator

36   HP   High pressure

37   HT   Hot tank

38   HTF   Heat transfer fluid

39   HX   Heat exchanger

40   IHX   Indirect heat exchanger

41   LCF   Low Cycle Fatigue

42   LP   Low pressure

43   PB   Power block

44	PI	Proportional-Integral
45	PTPP	Parabolic trough power plant
46	RH	Re-heater
47	SF	Solar field
48	SGS	Steam generator system
49	SH	Super-heater
50	SM	Solar multiple
51	ST	Steam turbine
52	TES	Thermal Energy Storage

53 **Symbols**

54	ITD	Inlet Temperature Difference	[°C]
55	$\dot{m}$	Mass flow	[kg/s]
56	p	Pressure	[bar]
57	T	Temperature	[°C]
58	t	Time	[s]
59	v_T	Allowable ramp-up rate/heating rate	[K/min]

60 *Subscripts*

61	f	fluid
62	max	maximum
63	min	minimum

1. Introduction

Concentrated solar power plants (CSPPs) are becoming more common in the renewable energy market. This trend is expected to rise in the upcoming years due to their key capability of being integrated with relatively cheap thermal energy storage (International Energy Agency, 2014). This feature makes it possible to decouple the energy generation from the solar input, making the power they can generate available at any time (Guedez et al., 2017). However, despite this characteristic feature, CSPPs are not currently designed for continuous operation, therefore they still experience daily start-ups and shut-downs. In order to maximize their performance from both technical and economical standpoints, increasing the flexibility of their dynamic performance is an important aspect which must be addressed (Topel et al., 2017). The rate at which a power plant can start up is limited by thermo-mechanical constraints, which may increase the time to reach the nominal load of the power plant. The receiver, the steam turbine and the steam generator system (SGS) are usually the most limiting components in this regard. While the receiver (Samanes and Garcia-Barberena, 2014) and steam turbine (Topel et al., 2017) have been examined in the literature, the steam generator has not been the focus of many studies .

Many CSPPs in use today have steam generators which were typically designed as conventional heat exchangers, not optimised for transient applications (Vant-Hull, 2012). As the industry mainly used designs from conventional power plants, their SGS responded inefficiently to sudden changes in incident solar radiation and equally poorly to repeated morning start-ups. This can cause failures in the component due to excessive thermal stresses, which may compromise the economic viability of the power plants. Although the industry is interested in optimising SGS designs for CSPPs (Pelagotti et al., 2014), there is little information on optimal heating rate requirements. In order to maximize the flexibility (i.e. to increase the responsiveness of the power plant to a change in the power load or in insolation), and both the peak and the baseline rate of electric power production, it is essential that all the components are able to start as quickly as possible and enable the CSPPs to quickly start harvesting the incoming solar radiation. On the other hand, there might be limiting factors for one component, which might reduce the required heating rate for another. For example, if the receiver or solar field are the limiting factors, there is no need for the SGS to be able to start up at a faster rate than that of the solar field (Ferruzza et al., 2017).

92   The SGS and steam turbine both start up at a rate that is governed by the need to limit thermal stresses

93   and low-cycle fatigue (LCF) (Pelagotti et al., 2014; Topel et al., 2017). Thick-walled components,

94   material properties and temperature gradients are the limiting factors. In the case of the steam generator,

95   the main constraining factors are the maximum allowable stresses in thick walled components such as the

96   steam drum, super-heater headers and T or Y junctions in the steam pipelines (Dzierwa and Taler, 2014;

97   Taler et al., 2015). Typically, the limiting component is the evaporator drum, which is designed as a large

98   diameter high pressure vessel, which must consequently have thick walls. The start-up procedure of the

99   component is intended to reach nominal conditions for temperature, pressure and mass flow rates as

100   rapidly as possible. In the case of the steam turbine, the shaft seal and blading clearances determine the

101   maximum allowable thermal expansion of the components, while the shaft thickness is the limiting factor

102   for thermal stress. As a general rule, the starting procedure of a steam turbine can be considered to have

103   three different phases: pre start-up heating, rolling up and loading up. During this procedure, the key

104   parameter which limits the heating rate is the difference in temperature between the incoming steam and

105   the metal of the turbine. In order to avoid excessive thermal stresses in this component it is desirable to

106   keep the temperature difference as low as possible (Spelling et al., 2012).

107   In previous studies, much attention is given to the thermal stress that limits the maximum heating rates of

108   these components, but little information is available about their impact on the performance of the overall

109   power plant. For instance, González-Gómez et al. (2017) analysed the thermo-mechanical stress in the

110   case of SGS for solar applications, but the study was performed at component level, without considering

111   the impact of such limitations on the performance of the power plant. The author also focused on design

112   and cost-based optimization of such components without considering the system perspective.

113   The abovementioned studies considered the limitation regarding either the steam generator or the turbine,

114   without addressing the interaction between the two (Dzierwa et al., 2016; Dzierwa and Taler, 2014; Taler

115   et al., 2015). It is of crucial importance to evaluate how much different constraints on the start-up

116   procedures of CSPPs affect their electric power production and whether significant differences occur

117   under different conditions. This information will indicate where to improve the operation of the power

118   plant and the design specifications for the components, from a thermo-mechanical point of view. Lastly,

119   the operational strategy of the power plant determines the number of start-ups and their typology (hot,

120   warm or cold start-ups) (Guedez et al., 2017; Spelling et al., 2012). For instance, if a CSPP operates

121 purely in solar-driven without fuel back-up, its start-up would mainly occur in the morning when the sun

122 is still rising. On the other hand, if a power plant is designed to work in peak load during a particular time

123 of the day (e.g. during evening hours, when the price of electricity is higher), the start-up would occur

124 when solar radiation or heat from the storage are readily available. From a start-up perspective (in the

125 absence of back-up fuels), this would mean different availability of heat input, hence different start-up

126 constraints.

127 The dynamic performance of parabolic trough power plants has been analysed previously (Almasabi et

128 al., 2015; Blanco et al., 2011; Conrado et al., 2017; Luo et al., 2015), although the models proposed deal

129 only with validation of the detailed component modelling of the solar field. Blanco et al. (2011)

130 presented a model of a parabolic trough power plant (PTPP) and validated it against experimental data,

131 but in this case the model of the power block was developed with a simplified correlation. Another

132 approach was presented by Abed et al. (2016), in which a detailed dynamic model in APROS (Advanced

133 Process Simulation Software) was validated against the operational data of Andasol II. The focus of the

134 study was to develop a detailed control strategy of the power plant by means of PI (Proportional-Integral)

135 controllers. The model presented did not focus on yearly performance but on daily control. None of these

136 studies considered start-up constraints due to thermo-mechanical limitations. In previous works such

137 constraints were usually analysed from a component perspective. For instance, Pelagotti et al. (2014)

138 described in detail a dynamic model of a steam generator, and carried out a low-cycle fatigue analysis.

139 The authors predicted the impact on the annual electricity production of PTPPs. Their calculations did not

140 take into account start-up schedules of steam turbines or rates of heat availability, nor yearly performance

141 evaluation of such power plants. A previous work by the authors (Topel et al., 2015) considered the

142 impact of the start-up rate of the steam turbine for solar tower direct steam generation; however , in this

143 work the start-up constraints of the steam turbine were not coupled with SGS constraints.

144 This paper presents an analysis of the effects of the thermal stress limitations of the steam generator

145 and steam turbine on the power plant start-up, and quantifies their impact on the economy of the system.

146 The study was performed for both solar-driven and peak-load conditions to emphasize on how different

147 constraints on starting up a steam generator have different impacts on the electric power production and

148 depend on how the plant is operated (Guedez et al., 2017). The paper also considers how differently sized

149   solar fields (in terms of solar multiple) affect the impact of the steam turbine and steam generator

150   constraints from an operational perspective.

151   In section 2 the paper presents the approach used for modelling the power plant. Secondly, it

152   summarizes the main limitation for the start-up of the steam generator and turbine and how such

153   constraints were implemented in the control logic for the overall model. In section 3, it presents the

154   evaluation of the impact of the constraints of the steam generator on the electric power production both in

155   peak-load and solar-driven together with a discussion on the results. Lastly section 4 outlines the

156   conclusions and final remarks.

157   **2. Methods**

158   Modelling was performed in DYESOPT, an in-house tool developed at KTH, Royal Institute of

159   Technology, Stockholm, which was developed for techno-economic modelling of CSP plants (Guedez et

160   al., 2017). The tool has been validated against Thermoflex, a commercially available software for power

161   plant performance estimation (Thermoflow, 2014), demonstrating a relative deviation between the results

162   of two software below 10 % in the case considered. As may be seen in Figure 1**,** the tool allows for both

163   steady-state design and dynamic simulation, and can make techno-economic calculations for different

164   assumed locations for the plant. The overall approach, as shown in Figure 1, can be linked to a multi-

165   objective optimizer (Guedez et al., 2017).
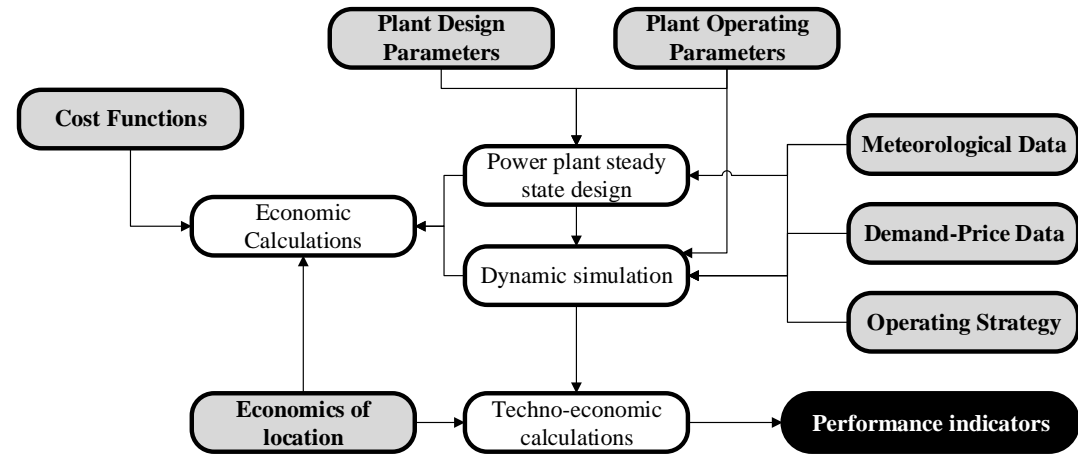

Figure 1: DYESOPT workflow diagram.

166   The model of the PTPP was implemented in the tool and validated as described in Ferruzza et al., (2015).

167   The author implemented the parabolic trough sizing methodology and the TRNSYS model in DYESOPT

168   and validated against data available in literature with a maximum error of -8.9 % (Ferruzza et al., 2017).

169 The model was further developed by including different operating strategies and the option of including

170 an air-cooled condenser (ACC). The consideration of ACCs is of topical interest, as many plants that are

171 currently under development or in the tender phase will be placed in desert areas. Having no direct access

172 to cooling water mandates the use of ACC in which the condensation of steam is achieved solely by air

173 cooling and parasitic electrical power consumption (Moore et al., 2013). The ACC model was previously

174 validated by Guedez et al. (2017).

175 **2.2 Steam generator start-up limitations**

176 The start-up procedure for a steam generator consists of bringing temperature, pressure and mass flow

177 rate to nominal values in each component of the system. As noted above, the rate at which this can be

178 done is highly dependent on thermo-mechanical limitations that are determined by their materials and

179 geometry. Previous studies have shown that the main limiting components during an SGS start-up are the

180 evaporator and super-heater, hence these two were considered in detail in the present study (Basaran,

181 2015; Taler et al., 2015). Another constraint which must be addressed is the occurrence of thermal shocks

182 that might occur if the HTF temperature is higher than the metal temperature by more than a critical

183 amount, as the material could then experience cracking and ultimately failure (Price, 2017). A limit on the

184 maximum allowable temperature difference is usually implemented in the control logic of the start-up

185 operation. Even though the minimum and maximum heating rates v_{Tmin} and v_{Tmax} for the required pressure

186 can be determined according to the norm DIN EN 12952-3 (CEN, 2012), the goal of the present study is

187 to determine the optimal range of values from a system perspective. The heating rates used to calculate

188 the permitted fluid temperature change were obtained using the following equation (Taler et al., 2015):

$$\frac{dT_{\mathrm{f}}}{dt} = \frac{p_{\max} \, v_{\mathrm{T_{min}}} - p_{\min} \, v_{\mathrm{T_{max}}}}{p_{\max} - p_{\min}} + \frac{v_{\mathrm{T_{max}}} - v_{\mathrm{T_{min}}}}{p_{\max} - p_{\min}} \, p(T_{\mathrm{f}}) \tag{1}$$

189 These equations express the rate at which the fluid temperature (T_{f}) can change depending on the pressure

190 of the fluid (minimum ($p_{\min}$) and maximum ($p_{\max}$)) and the minimum and maximum heating rates

191 which are dependent on the geometry, material properties and operating temperature and pressure. In an

192 evaporator, the water is at saturation point so the pressure and temperature are related. As a consequence,

193 the temperature of the fluid will be dependent on the pressure, and Equation (1) can be solved using a

194   Runge-Kutta method, assuming $T_f(t = 0) = T_0$. In the case of the super-heater, the fluid is not at

195   saturation conditions, the pressure is a function of time and determined by the evaporator conditions.

196   Simulations were carried out for different constraints on the evaporator and the super-heater. As discussed

197   by the authors in Ferruzza et al. (2015), an optimal heating rate constraint can be found for the super-

198   heater by assuming that it is 1.8 times higher than the evaporator limit. However, simulations were also

199   carried out using a 1.1 multiplier, to demonstrate the impact of this value and show how sensitive the

200   results are to this design parameter. Two main start-up schedules can be identified for the evaporator. In

201   the case of an evaporator with a drum configuration (natural or forced circulation), the minimum

202   allowable pressure of the steam turbine can be maintained overnight. Such a start-up routine will be

203   termed a hot start-up. However, when this is not possible (absence of steam drum or pressure vessel), the

204   pressure would not be maintained overnight and the evaporator would have to start up from ambient

205   pressure conditions. This will be termed a cold start-up. In order to study how different heating rate

206   routines will affect the start-up of the power plant, both hot and cold start-ups were included, making the

207   assumption that the overnight heat losses from the steam drum will be negligible. Observations from

208   existing power plants indicate that the overnight heat losses from the steam drum may be neglected due to

209   the large mass of water containing a high thermal inertia and experiencing a limited temperature drop.

210   **2.3 Steam turbine start-up schedule**

211   As for the SGS, the steam turbine start-up procedure is limited by the permissible temperature difference

212   between the metal surface and the steam. Different start-up schedules are defined by the manufacturer

213   based on the initial temperature of the turbine metal (or stand still time). The start-ups procedures are

214   classified as cold, warm or hot. A hot start-up would take only 8-10 % of the time it takes for a cold start-

215   up, while a warm start-up would take 45-50 % of that of a cold start-up (Topel et al., 2015). Figure 2

216   illustrates the three different start-up curves. The start-up procedure involves two phase which are

217   denoted for the cold case as the A-B and B-C lines which represent the rolling up and loading up of the

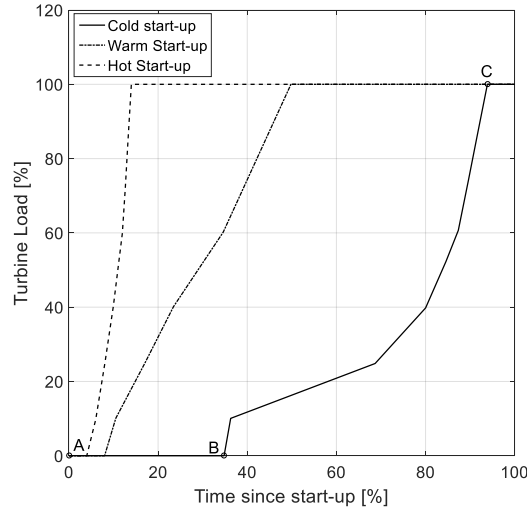218   turbine, respectively (Topel et al., 2015).

Figure 2: Cold, warm and hot steam turbine start-ups (Adapted from Topel et al., (2015)).

219 The start-up schedules were kept constant in order to focus mostly on the impact of the steam generator

220 on the overall performance of the power plant. The minimum allowable pressure was kept at 35 bar (as by

221 requirement of the steam turbine) and the rate at which pressure, mass flow rate and temperature could

222 rise were determined following the paper by. Schenk et al., (2015). During the running-up the mass flow

223 rate is kept at 5 % of the nominal value, while during the loading up the mass flow rate increases with a

224 rate determined directly by the steam turbine start-up routine depending on the metal temperature at

225 which the procedure begins. The different hot, warm and cold start-up curves presented in Figure 2 were

226 introduced in the model, depending on the metal temperature (Topel et al., 2015).

227 **2.4 Power plant modelling**

228 The plant layout considered in the paper is shown in Figure 3. The thick lines represent the HTF loop,

229 which is heated up by the parabolic trough (PT) mirrors, and either fed directly to the steam generator

230 (comprising an economizer (ECO), evaporator (EVA), super-heater (SH) and re-heater (RH)) or to heat-

231 up, through the indirect heat exchanger (IHX), the salts from the cold tank (CT) which are then pumped

232 to the hot tank (HT). The other cycle represents a conventional Rankine-reheat cycle with high pressure

233 (HP) and low pressure (LP) steam turbines (ST) an air-cooled condenser (ACC) and a deaerator (D).The

234 power plant was designed for the location of Seville, Spain, with a power output of 55 MWe gross,

235 according to Guedez et al. (2017) for the power block, Gilman et al. (2008) for the HTF cycle Lippke

236 (1995) and Dudley (1994) for the solar field. Firstly, the Rankine cycle was designed for the chosen gross

237   power, determining its efficiency and thermal input requirement. The size of the solar field was

238   determined accordingly and scaled considering the solar multiple (SM). Lastly, the thermal energy

239   storage (TES) mass was calculated to ensure the amount of hours desired to satisfy the thermal demand of

240   the power block. The design methodology was implemented in Matlab, while the yearly performance

241   dynamic model was developed in TRNSYS (University of Wisconsin Madison, 1975) in order to be

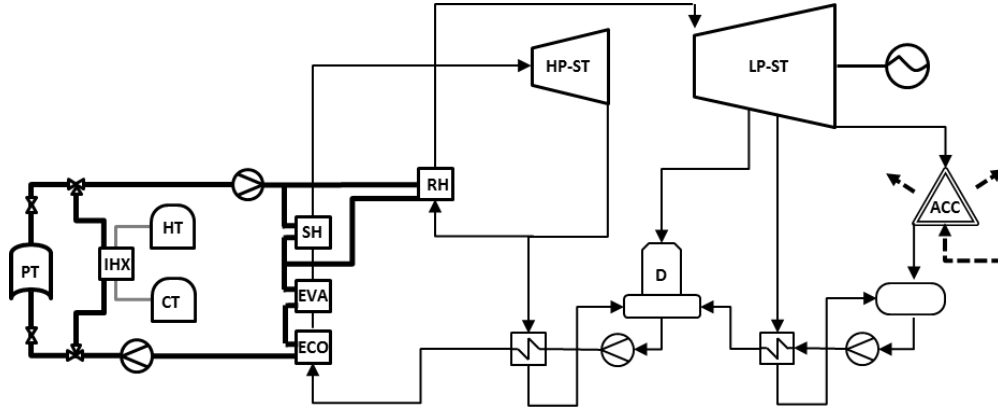242   implemented in DYESOPT.

Figure 3: Layout of the considered parabolic trough power plant integrated with indirect thermal energy storage and air cooled condenser.

243   The dynamic model of the power plant was integrated with a controller, which ran the start-up procedure

244   and applied the constraints to the steam generator and turbine. The logic of the controller is shown in

245   Figure 4. A similar strategy was applied when the power plant was operating either in solar-driven or

246   peak-load. In solar-driven, the start-up will occur in the morning as soon as the solar heat is available. In

247   this case, both the thermal shock and the thermal stresses (in the form of heating rates) are calculated and

248   a required HTF temperature is sent to the solar field. Afterwards, the steam temperature and pressure rise

249   accordingly, until the minimum allowable condition for superheated steam is reached. At this point the

250   steam turbine can start according to the start-up procedure. Similarly, for peak-load operation, the heating

251   rate constraints are calculated, from which a HTF temperature is obtained. However, as the plant operates

252   at specific times of the day, an optimal design is supposed to ensure that there is heat available to be

253   extracted from either the solar field or the thermal storage hot tank. If the thermal storage is used, the oil

254   temperature can be regulated by adjusting the salt mass flow rate. If HTF temperatures higher than the

255   allowable SGS HTF temperature occur, an attemperator may be used to reduce the temperature of the

256   thermal oil or the HTF may be mixed (if possible) with oil at a lower temperature, either from the solar

257   field loop or the SGS return line. One of the key differences between the two operation modes is the fact

258   that at peak-load the heat is readily available for the SGS and its constraints are the limiting factors, while

259   in solar-driven operation mode, the heat availability is dependent on the position of the sun and the size of
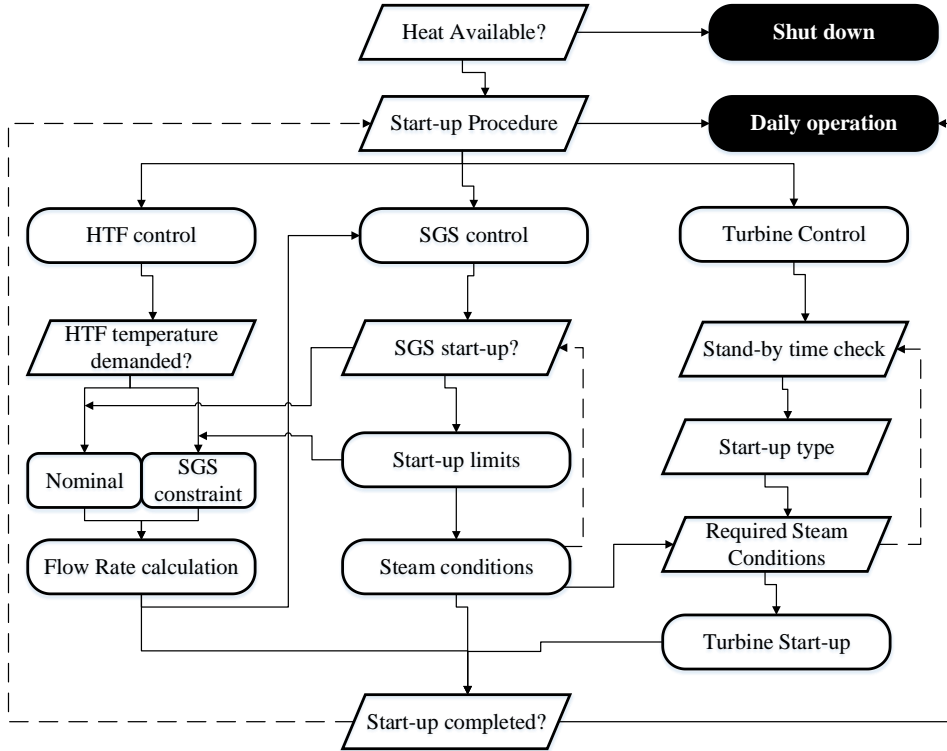
260   the solar field.

Figure 4: Control logic for the power plant during start-ups.

261   Once both the turbine and the steam generator have reached nominal operating conditions, the start-up

262   procedure is finished and the power plant enters daily operation. Part-load operation is taken into account

263   according to DLR (2006), if nominal heat input is not reached at the steam generator. The strategy

264   depicted in Figure 4 is applicable in both peak-load and solar-driven operation mode. Table 1 summarizes

265   the conditions for the two operational modes following Guedez et al. (2017).

Table 1: Summary of operation modes

Operation mode name	Condition
Solar-driven	Whenever radiation or TES are available
Peak-load	Only between 15-21 if heat input is available

266   The main design parameters and thermal performance indicators are listed in Table 2. It summarizes both

267   the parameters which were considered fixed and the ones that were allowed to vary for the purpose of the

268   analysis. The PTPP designed according to Table 2 served as a basis for an analysis of the impact of the

269   constraints. The SM and TES size for the peak-load case were chosen following Guedez et al. (2017). In

270   the solar-driven case the SM was varied to account for the impact of the solar field size while the TES

271   was kept at 10 h as this was a size that would still require warm turbine start-ups while allowing the plant

272   to operate in the evening even in winter periods. The 15-21 time operation was chosen according to

273   Guedez et al. (2017). However, in Guedez et al. (2017) the price of electricity in the suggested location

274   was higher than zero even between 5 and 17. The study considered only peak price hours, in order to

275   remove the influence of the solar field on the SGS. This means that the heat provided to the steam

276   generator comes directly either only from the TES or from the combination of the TES and SF, in case it

277   cannot come directly from the solar input. If the DNI is high enough the PT has already gone through its

278   start-up phase and could potentially provide nominal heat input to the steam generator. This makes it

279   possible to focus on how the constraints of the evaporator and super-heater affect the performance of the

280   power plant if electricity production was postponed to a particular time of the day.

Table 2: Summary of design parameters

Operation mode name	Units	Peakload case	Solar-driven case
SM	[-]	1.1	1.5-3
Gross Power	[MW]	55	55
TES capacity	[h]	5	10
Inlet HP/LP pressure	[bar]	100/16.7	100/16.7
Nominal condensing pressure	[bar]	0.06	0.06
SF HTF maximum temperature	[°C]	393	393
Nominal turbine inlet temperature	[°C]	378	378

281   **3 Results and discussion**

282   The impact of the start-up constraints was investigated and the performance of the power plant under

283   different limitations is presented in this section. Both peak-load and solar-driven operation were analysed.

284   For both of these modes, the start-up constraint of the steam generator was analysed for the cases shown

285   in Table 3.

Table 3: Summary of the respective parameters for the four different cases analyzed.

Case Name	Case 1 a/b	Case 2 a/b	Case 3 a/b	Case 4 a/b
Average evaporator heating rate [K/min]	3-12	3-12	3-12	3-12
Super-heater heating rate multiplier [K/min]	1.1/1.8	1.1/1.8	1.1/1.8	1.1/1.8
Start pressure [bar]	35	1	35	1
Thermal shock ΔT [K]	63	63	63	63
Operation strategy	peakload	peakload	solar-driven	solar-driven

286   The lower threshold for evaporator constraints was chosen as a reference, representing a slow start-up of

287   the SGS system (Pelagotti et al., 2014). This constraint can be considered as representative of a steam

288   generator system based on a kettle-reboiler type evaporator (González-Gómez et al., 2017). The higher

289   threshold was chosen as a potential improvement compared with the designs of header and coil

290   geometrical configurations already available in industry (Aalborg CSP, 2015). The cases are also

291   considering different start-up strategies for the steam generator. If a hot start-up is available (Case 1 and

292   Case 3 respectively), it means that the minimum allowable pressure of the turbine is kept at the steam

293   drum. In the case of a cold start-up (Case 2 and Case 4 respectively), the pressure starts from ambient

294   conditions.

295   **3.1 Peak-load case**

296   Figure 5 shows the results of the impact of the SGS heating rate constraints on the yearly electricity

297   production for the cases presented in Table 3. The graph indicates that for a hot start-up, the potential

298   improvement in Case 1 is 1.54 % (0.9 GWhe) for Case 1a. For cold start-ups of the evaporator, the

299   potential increases to 12.5 % (6.3 GWhe). Higher impacts were found for Cases 1b and 2b, when lower

300   SH heating rate multipliers were chosen, the potential for improvement being as high as 3.6 % and 25 %.

301   In the first cases, the evaporator was the main limiting factor during the start-up, while in the latter the

302   limitations imposed on the super-heater delayed the initial phase of the turbine start-up, making the

303   impact of the procedure more significant in terms of electricity production. These findings demonstrate

304   the importance of a properly designed and operated super-heater while starting up the SGS. The results of

305   Case 1a suggest that for hot evaporator start-ups it is possible to identify an optimal range of heating rate

306   constraints around 7-8 K/min. Beyond this threshold, no significant increase in power production was

307   observed, making it unnecessary to go above this design point. This is mainly due to the fact that even

308   though the SH could reach its nominal operating condition at faster rates, the turbine would still have to

309   be operated so as to respect its thermal limitations. This underlines how significant it is to consider both

310   components when optimising the total system design to respect thermo-mechanical constraints. If a faster

311   start-up rate was achievable for the steam turbine, then higher start-up constraints would be required for

312   the steam generator. For a cold start-up of an evaporator, higher start-up rates would always imply greater

313   electricity production for both a slow and a fast super-heater. In fact, the pressure that could be

314   maintained overnight was well below the minimum allowable pressure for the steam turbine, requiring

315   that SGS covers a larger temperature gradient, in turn postponing the beginning of the steam turbine start-
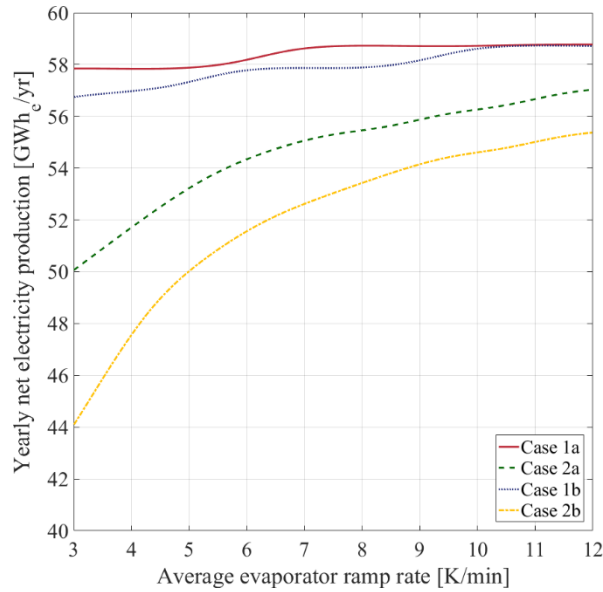
316   up.

14

Figure 5: Impact of the evaporator heating rate constraints on the net electricity production for a peak-load operating strategy.

317   Figures 6a and 6b show respectively the steam temperature during a two day period and the net

318   electricity output for case 1a. The two different lines refer to a slow (3 K/min) and a fast (12 K/min) SGS

319   configuration. Figures 7a and 7b show the same variables but for case 2a. The results illustrated in Figure

320   5 may better understood by looking at Figures 6 and 7. In the first two, it may be seen that even if the

321   evaporator start-up rate is 4 times higher than in the slow case, the impact on the net power output is

322   barely noticeable (a close up is shown in the left part of the graph). This means that every day the

323   beginning of the steam turbine start-up procedure is delayed by 6 minutes. In case 2, on the other hand, if

324   the steam pressure is not maintained overnight, the delay is more significant and observable. In this case

325   the steam turbine would experience a delay of as much as 30 minutes, making the SGS a bottleneck for

326   the start-up procedure. These considerations indicate that the presence of a pressure vessel (in the form of

327   a steam drum in this case) is important, to make the start-up procedure as effective as possible.
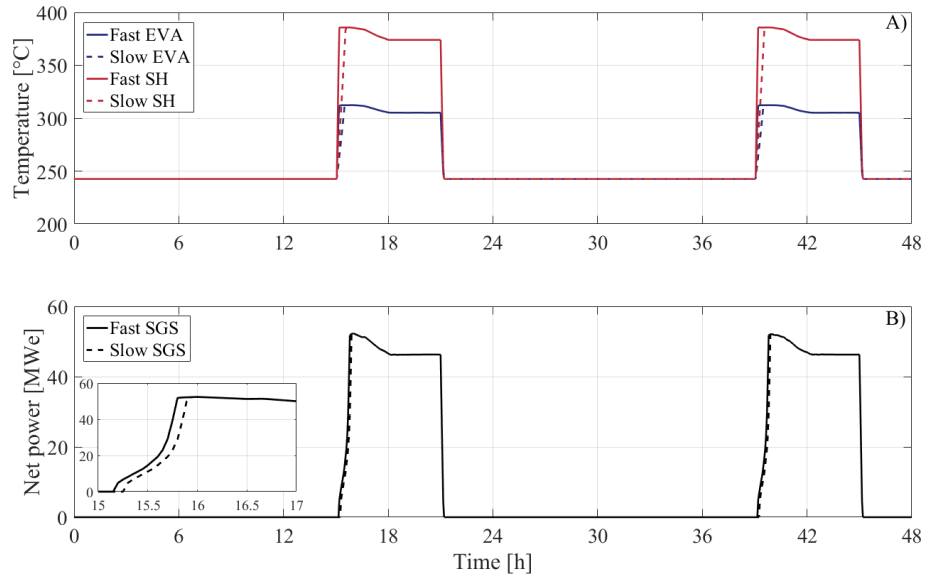
Figure 6: Comparison of a two-day performance between a slow and a fast evaporator during a hot start-up for a peak-load operating strategy case. A) Evaporator and super-heater temperatures, B) Net power output.
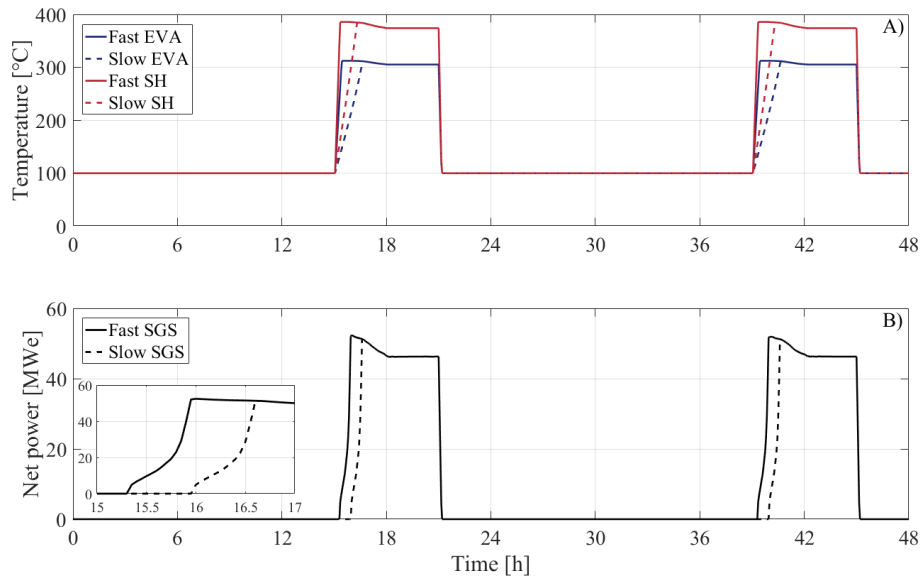
328

Figure 7: Comparison of a two-day performance between a slow and a fast evaporator during a cold start-up for a peak-load operating strategy case. A) Evaporator and super-heater temperatures, B) Net power output.

329

3.2 Solar-driven case

331   Figure 8 illustrates an analysis similar to the one described in section 3.1 but for a solar-driven

332   operational strategy. The reference case adopted was for a SM equal to 2, being a representative value for

333   existing power plant configurations like Andasol (Ferruzza et al., 2017). Following a similar

334   consideration as before, if only hot evaporator start-ups are considered, the results indicate that the

335   potential for improvement of the net electricity production is as low as 0.27 % (0.56GWhe), while for

336   cold start-ups, this impact increases to a maximum of 2.3 %. As in the previous case, if the super heater is

337   not operated or designed optimally, the maximum potential improvement is 4.65 % for cold start-ups.
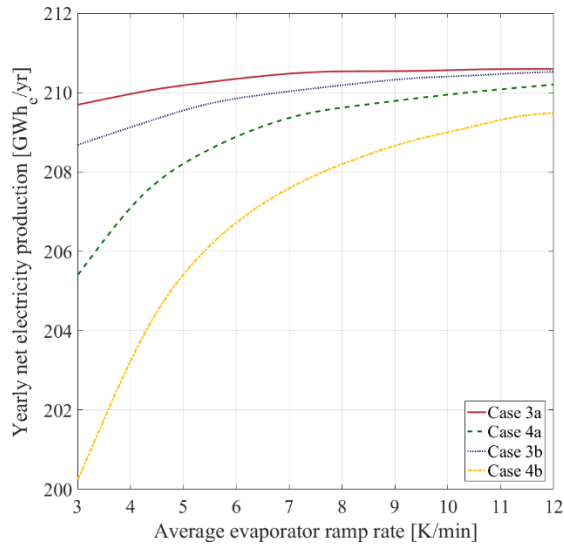

Figure 8: Impact of the evaporator ramp rate on the net electricity production for a solar-driven operating strategy case, considering a solar multiple equal to 2.
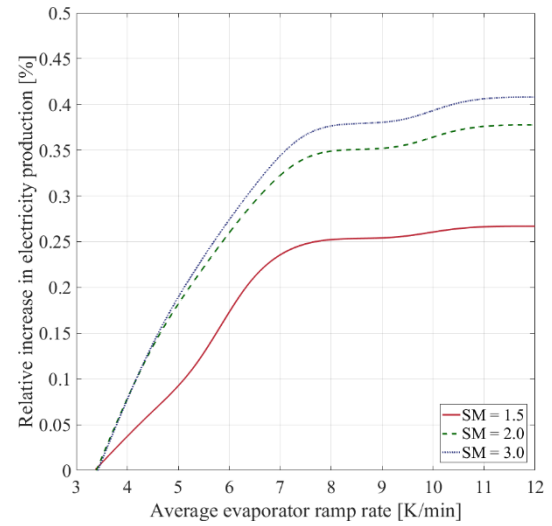
Figure 9: Sensitivity to the solar field size on the impact of the evaporator ramp rate constraints for a solar-driven operating strategy case.

338   Figure 9 illustrates the relative increase in electricity production for different Solar Multiple (SM) cases.

339   The figure suggests that the impact of the start-up constraints on the steam generator is considerably

340   affected by the size of the solar field. It may be seen that by doubling the size of the solar field from a SM

341   of 1.5 to 3.0, the relative increase can be improved from a maximum of 0.28 % to 0.41 %. However, the

342   impact is not very important in the economy of the power plant. Figure 10 illustrates the development of

343   the solar field thermal output and thermal input to the SGS and may suggest some reasons for this low

344   improvement. The close-up in the figure shows that in the morning, the heat input to the SGS follows the

345 same trend as the solar field output, as no storage is available. This means that to reach the nominal

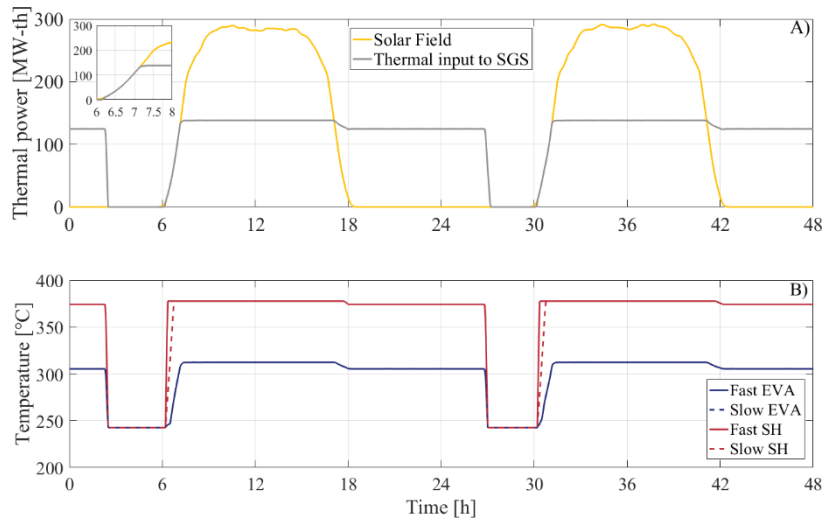346 operating condition of thermal output takes roughly 1 hour.

Figure 10: Comparison of a two-day performance between a slow and a fast evaporator during a hot start-up for a solar-driven operating strategy case. A) Thermal power at solar field and input to the steam generator system, B) Evaporator and Super-heater temperatures

347 The pressure at the SGS follows a similar trend, as it is proportional to the heat input to the evaporator.

348 Hence the start-up at the evaporator is no longer limited by its thermo-mechanical constraints but more by

349 the heat available from the solar field. This is directly shown in in the lower part of Figure 10. It may be

350 seen that in both the slow and fast cases, the temperature at the evaporator (and therefore the pressure, as

351 it is at saturation point), are not two separate lines but they overlap. The only limiting component from a

352 thermo-mechanical standpoint is therefore the super-heater, resulting in only negligible differences in

353 power production. In these cases the steam reaches the minimum allowable conditions at a later stage,

354 delaying the start-up of the turbine.

355 **4. Conclusions**

356 A detailed analysis was used to illustrate the impact of the SGS constraints during the start-up procedure

357 of a PTPP. To achieve this, an existing detailed model of a PTPP that had previously been developed by

358 the authors was extended to allow the simulation of two different operating strategies, namely peak-load

359 and solar-driven operation. The model was also extended by the addition of an air-cooled condenser. A

360 simulation tool was used to apply the start-up constraints of both the steam generator and the turbine. The

361 model was integrated with an existing tool for the dynamic performance evaluation of power plants

362 (DYESOPT).

363 The results suggest that for peak-load operation, by changing the constraints of the steam generator from

364 3 K/min to 12 K/min, the potential improvement in total net electricity output is 1.5 %. It was shown that

365 being able to maintain the minimum allowable turbine pressure overnight would be highly beneficial as it

366 makes it possible to start the steam turbine in the most efficient way. The optimal range of maximum

367 allowable heating rate for the evaporator was found to be about 7-8 K/min, designing a component with

368 higher constraints would provide no benefit for the economy of the power plant. For solar-driven

369 operation, the results indicate that for a solar field design with a SM equal to 2, the potential improvement

370 of electricity production is as low as 0.27 %. This figure might increase if the SF is further oversized, but

371 only to 0.41 %. The main limiting factor during start-ups is the amount of heat available in the solar field.

372 As the solar field can only provide nominal operating power to the SGS after 1 hour, the pressure at the

373 evaporator cannot achieve its nominal value before that time, so the heating rate will be slower than the

374 maximum limits in most start-up procedures. As a general conclusion, the results indicate that raising the

375 maximum allowable evaporator constraints would not proportionally increase the yield of the power

376 plant, as their effect is limited, either by other constraints at the steam turbine or at the solar field. It is

377 therefore clear that the interaction among the three components is crucial when optimising the thermo-

378 mechanical design of an SGS.

379

380 **References**

381 Abed, W., Al-maliki, K., Alobaid, F., Kez, V., Epple, B., 2016. Modelling and dynamic simulation of a

382   parabolic trough power plant. J. Process Control 39, 123–138.

383   https://doi.org/10.1016/j.jprocont.2016.01.002

384 Almasabi, A., Alobaidli, A., Zhang, T.J., 2015. Transient characterization of multiple parabolic trough

385   collector loops in a 100 MW CSP plant for solar energy harvesting. Energy Procedia 69, 24–33.

386   https://doi.org/10.1016/j.egypro.2015.03.004

387 Basaran, I., 2015. A Comprehensive Study of the Imposed Limitations on Concentrating Solar Power

388   Plant Start-up Speeds. MSc, Thesis. Royal Institute of Technology (KTH), Stockholm.

389 Blanco, D., Luis, A., Garcı, I.L., 2011. Performance model for parabolic trough solar thermal power

390   plants with thermal storage : Comparison to operating plant data. Sol. Energy 85, 2443–2460.

391   https://doi.org/10.1016/j.solener.2011.07.002

392 CEN, 2012. Water-tube boilers and auxiliary installations - Part 3: Design and calculation for pressure

393   parts of the boiler. Brussels.

394 Conrado, L.S., Rodriguez-pulido, A., Calderón, G., 2017. Thermal performance of parabolic trough solar

395   collectors. Renew. Sustain. Energy Rev. 67, 1345–1359. https://doi.org/10.1016/j.rser.2016.09.071

396 DLR, 2006. A TRNSYS Model Library for Solar Thermal Electric Components (STEC), Reference

397   manual.

398 Dudley, V., 1994. SEGS LS-2 Solar Collector. Test Results. Sandia National Laboratories. Albuquerque,

399   New Mexico.

400 Dzierwa, P., Taler, D., Trojan, M., Taler, J., 2016. Evaporator Heating with Optimum Fluid Temperature

401   Changes. Procedia Eng. 157, 29–37. https://doi.org/10.1016/j.proeng.2016.08.334

402 Dzierwa, P., Taler, J., 2014. Optimum Heating of Pressure Vessels With Holes. J. Press. Vessel Technol.

403   137, 11202. https://doi.org/10.1115/1.4027584

404   Ferruzza, D., Topel, M., Basaran, I., Laumert, B., Haglind, F., 2017. Start-Up Performance of Parabolic

405   Trough Concentrating Solar Power Plants, in: AIP Conference Proceedings 1850. pp. 1–9.

406   https://doi.org/10.1063/1.4984542

407   Gilman, P., Laboratory, N.R.E., Laboratories, S.N., 2008. Solar advisor model user guide for version 2.0.

408   Technical Report.

409   González-Gómez, P.Á., Gómez-Hernández, J., Briongos, J.V., Santana, D., 2017a. Thermo-economic

410   optimization of molten salt steam generators. Energy Convers. Manag. · 146, 228–243.

411   https://doi.org/10.1016/j.enconman.2017.05.027

412   González-Gómez, P.Á., Petrakopoulou, F., Briongos, J.V., Santana, D., 2017b. Steam generator design

413   for solar towers using solar salt as heat transfer fluid, in: AIP Conference Proceedings. pp. 1–8.

414   https://doi.org/10.1063/1.4984363

415   Guedez, R., Topel, M., Ferragut, F., Callaba, I., Perez-segarra, C.D., 2017. A Methodology for

416   Determining Optimum Solar Tower Plant Configurations and Operating Strategies to Maximize

417   Profits Based on Hourly Electricity Market Prices and Tariffs. Sol. Energy Eng. 138, 1–12.

418   https://doi.org/10.1115/1.4032244

419   International Energy Agency, 2014. Technology Roadmap, Solar Thermal Electricity. Paris.

420   Lippke, F., 1995. Simulation of the Part-Load Behavior of a 30 Mwe SEGS Plant. Report. Sandia

421   National Laboratories. Albuquerque, New Mexico.

422   Luo, N., Yu, G., Hou, H.J., Yang, Y.P., 2015. Dynamic modeling and simulation of parabolic trough solar

423   system, in: SolarPACES 2014. pp. 1344–1348. https://doi.org/10.1016/j.egypro.2015.03.137

424   Moore, J., Grimes, R., O'Donovan, A., Walsh, E., 2013. Design and testing of a novel air-cooled

425   condenser for concentrated solar power plants. Energy Procedia 49, 1439–1449.

426   https://doi.org/10.1016/j.egypro.2014.03.153

427   Pelagotti, L., Sørensen, K., Condra, T.J., Joseph, T., Franco, A., 2014. Modelling of a Coil Steam

428   Generator for CSP applications $, in: Proceedings of the 55th International Conference on

429   Simulation and Modelling.

430   Price, J.W.H., 2017. Thermal Shock Cracking : Design and Assessment Guidelines Thermal Shock

431   Cracking : Design and Assessment Guidelines. J. Press. Vessel Technol. 129, 125–132.

432   https://doi.org/10.1115/1.2389029

433   Samanes, J., Garcia-barberena, J., 2014. A model for the transient performance simulation of solar cavity

434   receivers. Sol. Energy 110, 789–806. https://doi.org/10.1016/j.solener.2014.10.015

435   Schenk, H., Dersch, J., Hirsch, T., Polklas, T., 2015. Transient Simulation of the Power Block in a

436   Parabolic Trough Power Plant. Proc. 11 Int. Model. Conf. 605–614.

437   https://doi.org/10.3384/ecp15118605

438   Spelling, J., Jöcker, M., Martin, A., 2012. Annual performance improvement for solar steam turbines

439   through the use of temperature-maintaining modifications. Sol. Energy 86, 496–504.

440   https://doi.org/10.1016/j.solener.2011.10.023

441   Taler, J., Weglowski, B., Taler, D., Sobota, T., Dzierwa, P., Trojan, M., Madejski, P., Pilarczyk, M.,

442   2015. Determination of start-up curves for a boiler with natural circulation based on the analysis of

443   stress distribution in critical pressure components. Energy 92, 153–159.

444   https://doi.org/10.1016/j.energy.2015.03.086

445   Thermoflow, 2014. Thermoflex Modular Program for Thermal Power Sys- tems [WWW Document].

446   URL www.thermoflow.com (accessed 11.22.17).

447   Topel, M., Genrup, M., Jöcker, M., Spelling, J., Laumert, B., 2017. Operational Improvements for Startup

448   Time Reduction in Solar Steam Turbines. Sol. Energy Eng. 137, 1–8.

449   https://doi.org/10.1115/1.4028661

450   Topel, M., Guédez, R., Laumert, B., 2015. Impact of Increasing Steam Turbine Flexibility on the Annual

451 Performance of a Direct Steam Generation Tower Power Plant. Energy Procedia 69, 1171–1180.

452 https://doi.org/10.1016/j.egypro.2015.03.196

453 University of Wisconsin Madison. Solar Energy Laboratory., 1975. TRNSYS, a transient simulation

454 program. Madison, Wis. : The Laboratory, 1975.

455 Vant-Hull, L.L., 2012. Central tower concentrating solar power (CSP) systems, Concentrating Solar

456 Power Technology: Principles, Developments and Applications. Woodhead Publishing Limited,

457 Houston. https://doi.org/10.1016/B978-1-84569-769-3.50008-X

458 Aalborg CSP, 2015. Aalborg CSP Steam Generator. URL

459 http://www.aalborgcsp.com/quickmenu/brochures/ (accessed 8.3.17).

460